Propagation of thermal waves across a wedge

Agustín Salazar and Arantza Mendioroz

Citation: J. Appl. Phys. **112**, 063511 (2012); doi: 10.1063/1.4752413
View online: http://dx.doi.org/10.1063/1.4752413
View Table of Contents: http://jap.aip.org/resource/1/JAPIAU/v112/i6
Published by the American Institute of Physics.

Propagation of thermal waves across a wedge

Agustín Salazar[a] and Arantza Mendioroz
Departamento de Física Aplicada I, Escuela Técnica Superior de Ingeniería, Universidad del País Vasco UPV/EHU, Alameda Urquijo s/n, 48013 Bilbao, Spain

(Received 12 May 2012; accepted 15 August 2012; published online 19 September 2012)

Photothermal techniques have been widely developed to study the thermal properties and to detect buried defects of samples with flat parallel surfaces. In the last years, there has been a growing interest in the application of photothermal techniques to samples with non-flat surfaces, as is the case of rods, tubes, and balls. The aim of the present work is to study the propagation of thermal waves across wedge samples. We have considered plane illumination (launching plane thermal waves) as well as Gaussian illumination (producing spherical thermal waves). We focus on the behavior of the front and rear surface temperatures, which is recorded using lock-in infrared thermography. This work is aimed at expanding the use of photothermal techniques for the quantitative characterization of wedge samples, as is the case of gear, blades, screws, and other hardware tools. © *2012 American Institute of Physics*. [http://dx.doi.org/10.1063/1.4752413]

I. INTRODUCTION

Photothermal techniques are based on the generation and detection of thermal waves in the sample under study. Thermal waves are generated in a material after the absorption of an intensity modulated light beam. These highly damped thermal waves propagate through the material and are scattered by buried heterogeneities and by the sample surfaces. Different photothermal setups have been developed to detect these thermal waves and therefore to retrieve information on the thermal properties and internal structure of the material: Infrared thermography, photopyroelectric, mirage effect, photothermal reflectance, etc.[1]

For decades, research in photothermal techniques has been restricted to samples with flat parallel surfaces. In the last years, several studies on the propagation of thermal waves in samples with cylindrical[2–4] and spherical[5–7] shape have been published. These works proposed methods to measure the radial thermal conductivity and diffusivity of homogeneous rods, tubes, and spheres using photothermal techniques.

The aim of the present work is to study the propagation of thermal waves across wedge samples. The scattering of thermal waves by a 90° corner has been already studied.[8–11] It was found that close to the corner of the sample the amplitude of the thermal wave increases while its phase decreases. In this work, we complete the above mentioned researches by studying the behavior of thermal waves across wedges of selected angles. We have studied the effect of a plane illumination (launching plane thermal waves) as well as the effect of a Gaussian illumination (launching spherical thermal waves). We focus on the behavior of the front and rear surface temperatures, which is recorded in a non-contact manner by an infrared video camera. Measuring the front surface temperature is well suited to analyze the presence of subsurface defects. On the other hand, from the back surface temperature the thermal properties of the wedge can be retrieved.

This work is aimed at expanding the use of photothermal techniques for the quantitative characterization of wedge samples, representing common shapes of parts used in industrial mechanical devices as gears, axes, blades, screws, and other hardware tools.

II. THEORY

First, we study the propagation of plane thermal waves across a wedge of arbitrary angle. Then, we extend the research to spherical thermal waves.

A. Plane illumination

In this subsection, we study an opaque wedge of angle α illuminated by a plane light beam whose amplitude is modulated at a frequency f ($\omega = 2\pi f$). Its cross-section is given in Fig. 1(a). Adiabatic boundary conditions at the surfaces are assumed. Let us start by considering a point-like illumination of power P_o, modulated at a frequency f and located at coordinates $(x_o,0,z_o)$ in a homogeneous and semi-infinite medium ($y<0$). The temperature oscillation at any point (x,y,z) of the material is given by[12]

$$T(x,y,z) = \frac{P_o(1-R)}{4\pi K}\frac{e^{-qr}}{r}, \tag{1}$$

where $r = \sqrt{(x-x_o)^2 + y^2 + (z-z_o)^2}$, $q = \sqrt{i\omega/D}$ is the thermal wave vector, D is the thermal diffusivity, K is the thermal conductivity, and R is the surface reflectivity at the illumination wavelength. Equation (1) represents a highly damped spherical thermal wave generated at $(x_o,0,z_o)$. The temperature oscillation when the material is illuminated by a modulated plane source located at the semi-plane $y=0$ and $x>0$ is obtained by integrating Eq. (1) over that semi-plane

$$T(x,y,z) = \frac{I_o(1-R)}{4\pi K}\int_0^\infty dx_o \int_{-\infty}^{\infty} \frac{e^{-qr}}{r} dz_o, \tag{2}$$

where I_o is the intensity (W/m^2) of the illumination.

[a]E-mail: agustin.salazar@ehu.es.

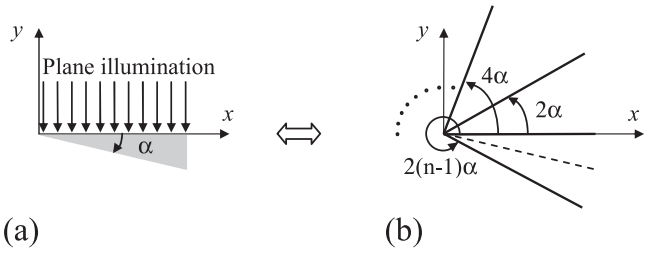

FIG. 1. (a) Cross-section of a wedge illuminated by a plane light beam. (b) Equivalent geometry after applying the image theorem.

Due to the adiabatic boundary conditions at the sample surfaces, the real geometry shown in Fig. 1(a) can be analyzed by considering the configuration shown in Fig. 1(b). Note that the effect of the wedge walls is accounted for via the introduction of $n = \pi/\alpha$ image plane illuminations located at angles $2\alpha, 4\alpha, 6\alpha, \ldots, 2(n-1)\alpha$. It is worth mentioning that this image method is only valid for wedge angles verifying $\alpha = \pi/n$, with $n \in N$.[13] For wedge angles different from these, the method would give rise to an infinite (meaningless) number of images. Finally, the temperature oscillation at any point of the wedge is obtained by adding the contribution of the real plane illumination plus the $n-1$ image plane illuminations

$$T(x,y,z) = \frac{I_o(1-R)}{4\pi K} \sum_{p=0}^{n-1} \int_0^\infty dx_o \int_{-\infty}^\infty \frac{e^{-qr'}}{r'} dz_o, \qquad (3)$$

where

$$r' = \sqrt{[x\cos(2p\alpha) + y\sin(2p\alpha) - x_o]^2 + [-x\sin(2p\alpha) + y\cos(2p\alpha)]^2 + (z-z_o)^2}. \qquad (4)$$

To obtain Eq. (3), we have used the rotation of the coordinate axes around the z axis.

In the case of $\alpha = 180°$, which represents a semi-infinite sample ($y < 0$) whose semi-plane $x > 0$ is illuminated by a plane light beam while the semi-plane $x < 0$ is non illuminated, Eq. (3) reduces to

$$T(x,y,z) = \frac{I_o(1-R)}{4\pi K} \int_0^\infty dx_o \times \int_{-\infty}^\infty \frac{e^{-q\sqrt{(x-x_o)^2+y^2+(z-z_o)^2}}}{\sqrt{(x-x_o)^2+y^2+(z-z_o)^2}} dz_o. \qquad (5)$$

For $\alpha = 90°$, a right angle corner, Eq. (3) reduces to

$$T(x,y,z) = \frac{I_o(1-R)}{4\pi K} \int_{-\infty}^\infty dx_o \times \int_{-\infty}^\infty \frac{e^{-q\sqrt{(x-x_o)^2+y^2+(z-z_o)^2}}}{\sqrt{(x-x_o)^2+y^2+(z-z_o)^2}} dz_o = \left(\frac{I_o}{2Kq}\right) e^{-qy}, \qquad (6)$$

which represents a plane thermal wave, in agreement with the prediction of the image method stating that a right corner is equivalent to semi-infinite sample.

Figure 2 shows the simulation of the front surface temperature of a wedge illuminated by a plane light beam as a function of the normalized distance (x/μ) to the edge of the wedge, where $\mu = \sqrt{D/\pi f}$ is the thermal diffusion length. Figure 2(a) shows the behavior of the natural logarithm of the amplitude, Ln(T), and Fig. 2(b) that of the phase, ψ. Results for wedge angles $\alpha = 5°$, 15°, 45°, 90°, and 180° are shown. As can be seen, for $\alpha = 90°$ both Ln(T) and ψ have a flat behavior consistent with the plane thermal wave given by Eq. (6). For $\alpha < 90°$, the amplitude of the temperature increases as approaching the edge of the wedge, while the phase shows a dip. The smaller the wedge angle α the deeper the phase dip, until a minimum phase value of 98.5° is reached for an infinitesimal wedge angle. This result is consistent with the fact that far away from the edge the sample is thermally thick ($\psi = -45°$), while close to the edge the sample becomes thermally thin ($\psi = -90°$). The opposite behavior is found for $\alpha = 180°$: the amplitude of the

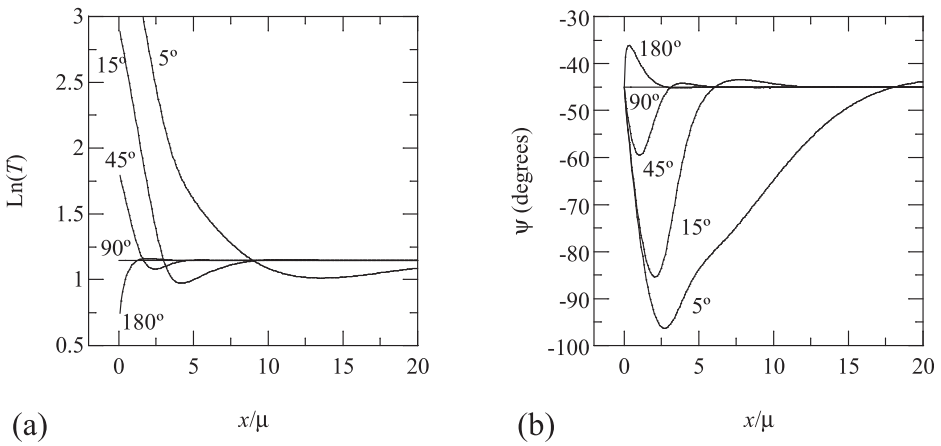

FIG. 2. Simulation of the front surface temperature of a wedge illuminated by a plane light beam as a function of the normalized distance (x/μ) to the edge of the wedge. (a) Natural logarithm of the amplitude, Ln(T), and (b) phase, ψ. Results for wedge angles $\alpha = 5°$, 15°, 45°, 90°, and 180° are shown.

temperature decreases as approaching the edge of the illumination, while the phase shows a peak.

Figure 3 shows the simulation of the rear surface temperature of a wedge illuminated by a plane light beam as a function of the normalized distance to the edge taken along the rear surface (d/μ). Results for wedge angles $\alpha = 2.5°$, 5°, 10°, 15°, 22.5°, and 45° are shown. For each α, the upper curve stands for Ln(T), while the lower curve represents ψ. As can be seen, as moving away from the edge of the wedge both Ln(T) and ψ become parallel straight lines whose slopes, m, verify $m = -\sin(\alpha)$. This means that the thermal diffusivity of the wedge can be obtained in a straightforward way from the slope m' of Ln(T) and ψ as a function of the distance to wedge (d): $D = -\frac{\pi f}{m'^2}\sin^2(\alpha)$.

B. Gaussian illumination

Now, we study the same opaque wedge as before but illuminated by a Gaussian light beam of radius a (at $1/e^2$ of the intensity) modulated at a frequency f. The center of the Gaussian spot is located at (b,0,0). The cross-section of the wedge is given in Fig. 4(a). Let us start by reminding that the temperature oscillation of a homogeneous and semi-infinite medium ($y < 0$) is given through the Fourier transform[14]

$$T(x,y,z) = \frac{I_o(1-R)}{4\pi K}\int_{-\infty}^{\infty}\int_{-\infty}^{\infty} e^{-i[(x-b)\delta+z\eta]}e^{-(\delta^2+\eta^2)a^2/8} \times \frac{e^{\beta y}}{\beta}d\delta d\eta, \tag{7}$$

where $\beta = \sqrt{\delta^2+\eta^2+q^2}$. By using the image theorem, the effect of the wedge walls is accounted for via the introduction of $n = \pi/\alpha$ image Gaussian spots located at angles 2α, 4α, 6α,…, $2(n-1)\alpha$ (see Fig. 4(b)). Accordingly, the temperature oscillation at any point of the wedge is obtained by adding the contribution of the real Gaussian spot and the $n-1$ image Gaussian spots

$$T(x,y,z) = \frac{I_o(1-R)}{4\pi K}\sum_{p=0}^{n-1}\int_{-\infty}^{\infty}\int_{-\infty}^{\infty} e^{-i\left\{\left[\left(x-b\cos(2p\alpha)\right)\cos(2p\alpha)+\left(y-b\sin(2p\alpha)\right)\sin(2p\alpha)\right]\delta+z\eta\right\}}e^{-(\delta^2+\eta^2)a^2/8} \times \frac{e^{\pm\beta\left[-\left(x-b\cos(2p\alpha)\right)\sin(2p\alpha)+\left(y-b\sin(2p\alpha)\right)\cos(2p\alpha)\right]}}{\beta}d\delta d\eta. \tag{8}$$

The sign in the exponential is either positive ($+\beta$) for $2p\alpha < \pi$ or negative ($-\beta$) for $2p\alpha \geq \pi$. In particular, for n even Eq. (8) consists of the addition of two terms, the first one with the summation running from 0 to $n/2-1$ with $\beta > 0$ and the second one with the summation running from $n/2$ to $n-1$ with $\beta < 0$. On the other hand, for n odd Eq. (8) can be written as the addition of two terms, the first one with the summation going from 0 to $(n-1)/2$ with $\beta > 0$ and the second one with the summation going from $(n+1)/2$ to $n-1$ with $\beta < 0$.

As a proof of self-consistency, it is worth mentioning that in the case of a 180° wedge, i.e., a semi-infinite sample, Eq. (8) reduces to Eq. (7).

For a tightly focused Gaussian beam ($a \approx 0$), if we move the Gaussian spot away from the wedge while recording the temperature at the center of the spot, constant amplitude and phase ($\psi = 0°$) are obtained. As the size of the spot is increased, an amplitude rise and a dip in phase as approaching the edge of the wedge are observed. This result is similar to that shown in Fig. 2 but with a much smaller contrast. Anyway, the case of a 90° wedge deserves some comments. For a point-like excitation ($a = 0$) or for a plane excitation ($a = \infty$), the theoretical model predicts a constant amplitude and phase, i.e., there is not any feature indicating the presence of that wedge. However, for intermediate beam sizes, small amplitude rise and phase decrease appear when

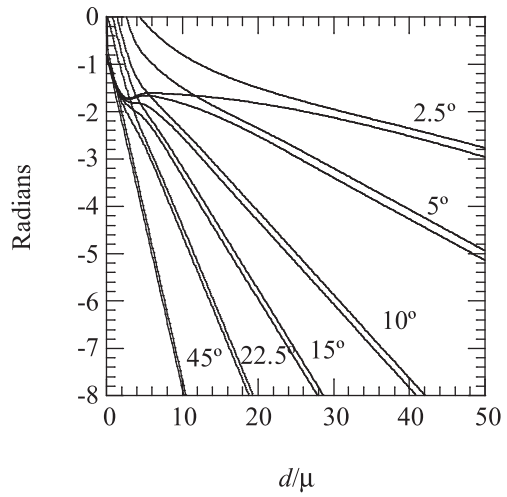

FIG. 3. Simulation of the rear surface temperature of a wedge illuminated by a plane light beam as a function of the normalized distance to the edge along the rear surface (d/μ). For each wedge angle, the upper curve stands for Ln(T), while the lower curve represents the phase.

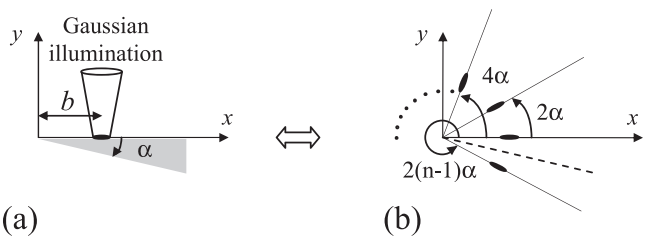

FIG. 4. (a) Cross-section of a wedge illuminated by a Gaussian light beam. (b) Equivalent geometry after applying the image theorem.

approaching the corner. This result agrees with previously reported works.[8,10]

Figure 5 shows the simulation of the rear surface temperature of a wedge illuminated by a Gaussian light beam of normalized radius $a/\mu = 0.1$, whose position is changed along the x axis. The rear surface temperature is computed at the opposite point with respect to the excitation, i.e., same x coordinate for both excitation and computing position. The abscissa in Fig. 5 represents the normalized distance to the edge taken along the back surface (d/μ). Results for wedge angles $\alpha = 5°$, 10°, 15°, 22.5°, and 45° are shown. For each α value, the upper curve stands for Ln(T), while the lower curve represents ψ. As can be seen, the result is similar to that found in Fig. 3 for a plane illumination. In fact, Ln(T) and ψ have the same slope as for plane illumination, verifying $m = -\sin(\alpha)$. The main difference is that the linear behavior starts closer to the edge than in the case of plane illumination.

Finally, Fig. 6 shows the simulation of the front surface temperature of a wedge as a function to the normalized distance to the edge (x/μ). The wedge is illuminated by a Gaussian light beam, with normalized radius $a/\mu = 0.1$, and centered at $b/\mu = 1$. Continuous lines represent the natural logarithm of the temperature amplitude multiplied by the normalized distance to the Gaussian spot center $Ln\left[\frac{|x-b|}{\mu}T\right]$ while dotted lines stand for temperature phase ψ. As can be observed, far away from the edge both the natural logarithm and the phase are parallel straight lines whose slope, m, verifies $m = -\sqrt{\pi f/D}$. This slope is independent of the wedge angle. This result is the same as that found in a semi-infinite slab. However, close to the edge there is an increase of the natural logarithm and phase, which is more pronounced as the wedge angle is smaller.

III. EXPERIMENTAL RESULTS AND DISCUSSION

To validate the theoretical predictions, wedges of different angles (90°, 20°, 15.4°, 10.2°, 7.2°, and 5.2°) made of AISI-304 stainless steel have been manufactured. In order to increase the light absorption and the infrared emissivity, a thin black paint layer of about 10 μm covered both surfaces of the wedge. The scheme of the experimental setup for a plane illumination is given in Fig. 7. The wedge is illuminated by a 50 W diode laser (808 nm) with "top hat" profile. Modulation of the laser power is accomplished by modulating the electric current feeding the laser driver. An optical fiber is used to direct the defocused laser beam onto the wedge surface. The surface temperature of the wedge is measured by an infrared video camera (SC7500-BB from FLIR). A 50 mm lens is used to collect the infrared emission from the sample surface. The sample is placed at the minimum possible working distance from the lens (about 25 cm). In this way, each pixel measures the average temperature over a square of 150 μm side on the wedge surface. The

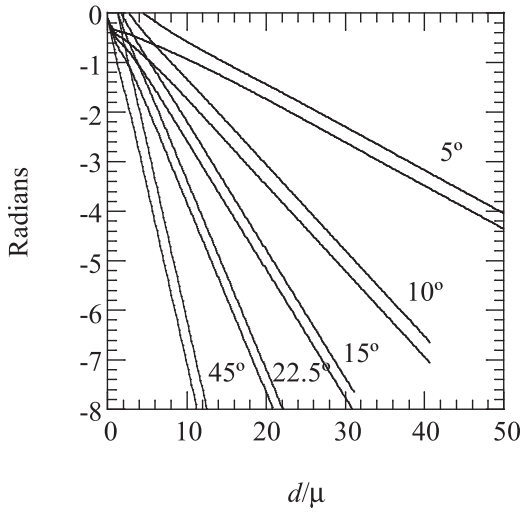

FIG. 5. Simulation of the rear surface temperature of a wedge illuminated by a Gaussian light beam of normalized radius $a/\mu = 0.1$, whose position is changed along the x axis. The rear surface temperature is computed at the opposite point with respect to the excitation. The abscissa represents the normalized distance to the edge taken along the back surface (d/μ).

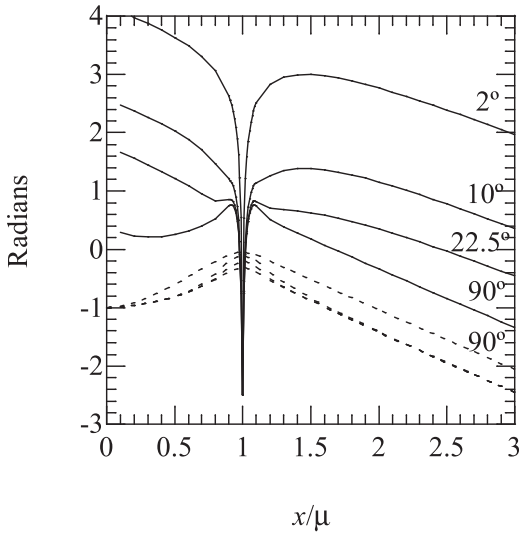

FIG. 6. Simulation of the front surface temperature of a wedge as a function to the normalized distance to the edge (x/μ). The wedge is illuminated by a Gaussian beam, with normalized radius $a/\mu = 0.1$, and centered at $b/\mu = 1$. Continuous lines represent the natural logarithm of the temperature amplitude multiplied by the normalized distance to the Gaussian spot center $Ln\left[\frac{|x-b|}{\mu}T\right]$ while dotted lines stand for temperature phase ψ.

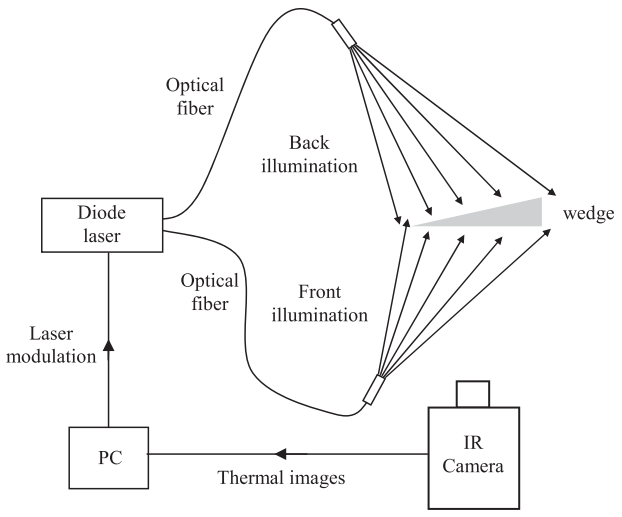

FIG. 7. Scheme of the infrared thermography setup. Note that there is only one optical fiber that illuminates the front or the back surface of the wedge.

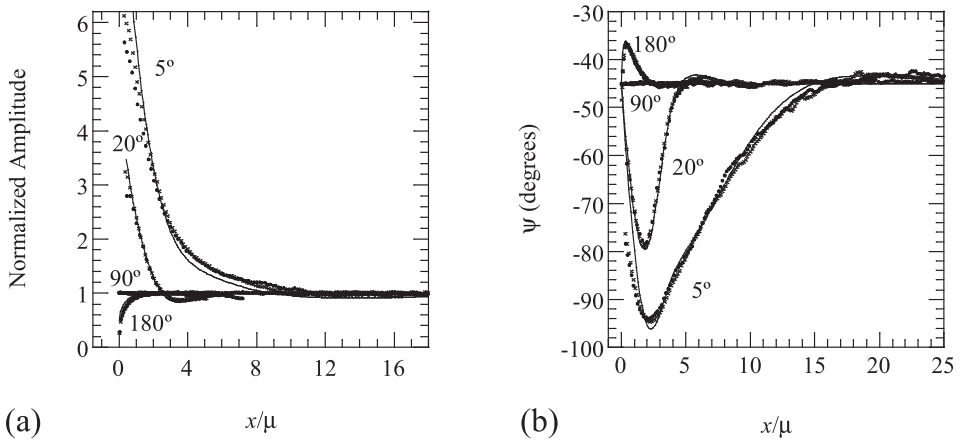

FIG. 8. Symbols are the experimental normalized amplitude (a) and phase (b) of the front surface temperature of a set of AISI-304 stainless steel wedges illuminated by a "top hat" laser as a function of the normalized distance (x/μ) to the edge. The continuous lines correspond to the theoretical prediction.

lock-in software provided with the camera gives the amplitude and phase of the oscillating temperature. To improve the signal to noise ratio, we record 4000 images for each experiment. As the noise level is inversely proportional to the square root of the total number of images,[15] we obtain a temperature noise level smaller than 1 mK.

Dots in Fig. 8 show the experimental normalized amplitude and phase of the front surface temperature of the wedges illuminated by the defocused diode laser (diameter around 5 cm) as a function of the normalized distance (x/μ) to the edge. Each wedge was measured at several modulation frequencies ranging from 0.12 Hz to 4.1 Hz. For the sake of clarity, only the results for some wedges and for two frequencies for each wedge are shown in Fig. 8. The continuous lines correspond to the theoretical predictions obtained from Eq. (3) and plotted in Fig. 2. As can be observed, they fit very well the experimental data. It is worth noting that the measurements corresponding to $\alpha = 180°$ are performed in a semi-infinite slab (far away from the sample edges) which is partially illuminated by the diode laser. The amplitude and phase of the temperature are recorded in the illuminated part of the sample as a function to the distance to the light edge.

Then, we have measured the amplitude and phase of the temperature at the back surface as a function to the distance to the wedge edge (d). Measurements have been performed in all the wedges we have prepared. For each wedge, measurements at frequencies in the range from 0.12 to 7.4 Hz have been carried out. For the sake of clarity, only some of the results are shown in Fig. 9. For each couple (α, f), the upper curve stands for Ln(T), while the lower curve represents the phase ψ. As can be seen, close to the edge Ln(T) and ψ have a nonlinear behavior. However, as we go away from the edge both Ln(T) and ψ become parallel straight lines with the slopes m' verifying $m' = -\sin(\alpha)\sqrt{\pi f/D}$. Using this expression, the thermal diffusivity of our set of AISI-304 stainless steel wedges has been obtained. All thermal diffusivity values fall in the range 3.8–4.1 mm^2/s, in agreement with the typical D values of AISI-304 that can be found in the literature, thus confirming the theoretical predictions.

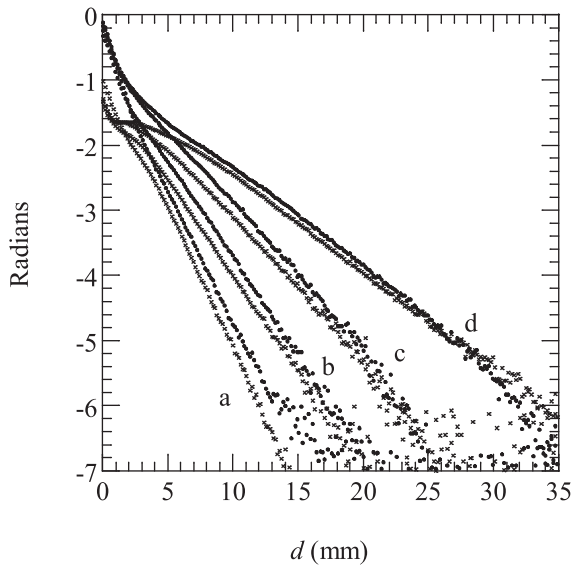

FIG. 9. Experimental measurements of the rear surface temperature of AISI-304 wedges illuminated by a "top hat" laser as a function of the distance to the edge taken along the back surface, d. (a) $\alpha = 20°$, $f = 1.90$ Hz, (b) $\alpha = 10.2°$, $f = 3.68$ Hz, (c) $\alpha = 5.2°$, $f = 7.36$ Hz, and (d) $\alpha = 5.2°$, $f = 3.68$ Hz. For each pair, the upper curve stands for Ln(T), while the lower curve represents the phase.

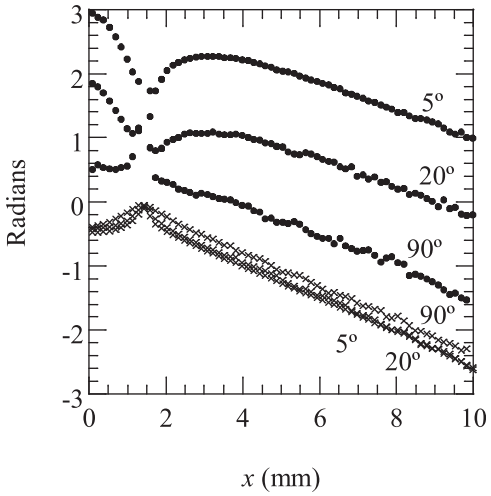

FIG. 10. Experimental results of the front surface temperature of AISI-304 wedges, illuminated by a focused Gaussian laser beam as a function of the distance to the edge x. The laser spot impinges at a distance $b = 1.4$ mm from the edge. Measurements are performed at $f = 70$ mHz. Dots represent $Ln[|x - 1.4|T]$ and crosses the phase.

For Gaussian illumination, we have used an acousto-optically modulated solid state laser (532 nm) focused onto the wedge surface by a spherical lens of 10 cm focal length. The surface temperature is measured by the same infrared video camera in lock-in mode. In Fig. 10, we show the IR termography measurements of the front surface temperature of the AISI-304 wedges, illuminated by that focused Gaussian spot as a function of the distance to the edge x. The laser spot impinges at a distance $b = 1.4$ mm from the edge. Measurements are performed at $f = 70$ mHz in order to have good enough resolution in the region between the laser spot and the edge. Dots represent $Ln[|x - 1.4|T]$ and crosses the phase. As predicted by the theory, when moving away from the edge, both the natural logarithm and the phase decrease linearly. However, when approaching the wedge edge the symmetry is broken in such a way that the phase, and especially the natural logarithm, shows a drastic increase of its values.

IV. SUMMARY AND CONCLUSIONS

In this work, we have developed a theoretical model to calculate the surface temperature of homogeneous wedge-shaped samples when illuminated by both plane and point-like modulated light beams. The calculations are subjected to two restrictions: first, adiabatic boundary conditions are assumed and second, angles α of the wedges must fulfil the condition $\alpha = \pi/n$. This is a strong limitation for large angles (90°, 60°, 45°, 36°,…), but not for small angles (3.6°, 3.53°, 3.46°,…) The predictions of the calculations have been validated by the results of infrared thermography experiments performed on stainless steel wedges of different angles, both with plane and point-like illumination.

One straightforward application of the method consists of obtaining the thermal diffusivity of wedge-shaped samples in an easy way. Furthermore, this study sets the grounds to further analyze the effect of the presence of defects in wedges on the surface temperature distribution. In the case of homogeneous flat samples, the surface temperature is constant (in amplitude and phase) when illuminated by an extended light beam. The presence of buried defects can be easily identified as a departure from this flat behavior of the surface temperature. In wedge samples, or near the corner of a flat sample, detection of defects is more complicated. Knowledge of the surface temperature distribution of homogeneous, defect-free wedges generated by plane or focused illumination is the first step in developing methods to assess the presence of buried defects, as cracks or delaminations close to the edges of a sample, from infrared thermography data.

ACKNOWLEDGMENTS

This work has been supported by the Ministerio de Ciencia e Innovación (MAT2011-23811), by Gobierno Vasco (IT351-10) and by UPV/EHU (UFI11/55).

[1]D. P. Almond and P. M. Patel, *Photothermal Science and Techniques* (Chapman and Hall, London, 1996).
[2]C. H. Wang, A. Mandelis, and Y. Liu, J. Appl. Phys. **96**, 3756 (2004).
[3]C. Wang, A. Mandelis, and Y. Liu, J. Appl. Phys. **97**, 014911 (2005).
[4]A. Salazar and R. Celorrio, J. Appl. Phys. **100**, 113535 (2006).
[5]A. Salazar, F. Garrido, and R. Celorrio, J. Appl. Phys. **99**, 066116 (2006).
[6]C. Wang, Y. Liu, A. Mandelis, and J. Shen, J. Appl. Phys. **101**, 083503 (2007).
[7]N. Madariaga and A. Salazar, J. Appl. Phys. **101**, 103534 (2007).
[8]L. C. Aamodt and J. C. Murphy, Appl. Opt. **21**, 111 (1982).
[9]K. Friedrich and H.-G. Walther, J. Appl. Phys. **70**, 4697 (1991).
[10]A. Sánchez-Lavega and A. Salazar, J. Appl. Phys. **74**, 536 (1993).
[11]A. Sánchez-Lavega and A. Salazar, J. Appl. Phys. **74**, 548 (1993).
[12]H. S. Carslaw and J. C. Jaeger, *Conduction of Heat in Solids* (Oxford University Press, Oxford, 1959), p. 263.
[13]A. Mandelis, *Diffusion-Wave Fields* (Springer-Verlag, New York, 2001), p. 410.
[14]A. Salazar, A. Sánchez-Lavega, A. Ocáriz, J. Guitonny, G. C. Pandey, D. Fournier, and A. C. Boccara, J. Appl. Phys. **79**, 3984 (1996).
[15]O. Breitenstein and M. Langenkamp, *Lock-in Thermography* (Springer, Berlin, 2003), p. 32.